

# e-CALLISTO FITS Analyzer: A Software Framework For CALLISTO Solar Radio Data

G.L.S.S. Liyanage,<sup>1\*</sup> J. Adassuriya,<sup>1</sup> K. P. S. C. Jayaratne<sup>1</sup> C. Monstein<sup>2</sup> and P. K. Manoharan<sup>3,4</sup>

<sup>1</sup>*Astronomy and Space Science Unit, Department of Physics, University of Colombo, Sri Lanka*

<sup>2</sup>*Istituto ricerche solari Aldo e Cele Daccò (IRSOL), Faculty of Informatics, Università della Svizzera italiana (USI), CH-6605 Locarno, Switzerland*

<sup>3</sup>*Heliophysics Science Division, NASA Goddard Space Flight Center, Greenbelt, MD 20771, USA*

<sup>4</sup>*The Catholic University of America, Washington, DC 20664, USA*

Accepted XXX. Received YYY; in original form ZZZ

## ABSTRACT

Solar radio bursts (SRBs) are important signatures of dynamic processes in the solar corona, including particle acceleration and shock propagation associated with solar flares and coronal mass ejections. Among the missions that report solar radio bursts within 24 hours, the e-CALLISTO archive is the largest and most successful, with more than 150 stations worldwide. The archive generates large volumes of FITS data that are often affected by radio-frequency interference and background noise. Irregular frequency setups in different stations are also a limitation of statistical analysis of SRBs. Each CALLISTO observation is a 15-minute frame, which often causes a single burst to split over multiple frames, making event-level analysis difficult. This work presents the e-CALLISTO FITS Analyzer, a unified, interactive, cross-platform application for processing and analyzing e-CALLISTO dynamic spectra on Windows, macOS, and Linux. The application supports time and frequency merging to produce a continuous spectrum, applies mean background subtraction with user-controlled threshold clipping, and isolates burst regions through an interactive polygon mask in the time–frequency plane. It also extracts the maximum-intensity backbone, allows interactive outlier removal, and performs power-law fitting to estimate drift rates and derive shock height and speed using the Newkirk model, including  $n$ -fold scaling. For a Type II burst observed by Arecibo Observatory on 2 March 2022, the analyzer yielded an average drift rate of  $-0.0400 \pm 0.0003$  MHz/s and an average shock speed of  $449 \pm 1$  km/s at a height of  $1.715 \pm 0.002 R_{\odot}$ . The e-CALLISTO FITS Analyzer supports more reproducible, event-focused SRB analysis and improves access to physically meaningful measurements from e-CALLISTO FITS data.

**Key words:** Solar radio bursts – Dynamic spectra – Type II bursts – e-CALLISTO – Drift rates – Shock speed

## 1 INTRODUCTION

Solar radio bursts (SRBs) are critical diagnostic indicators of dynamic processes in the solar corona, providing insights into particle acceleration and shock wave propagation associated with solar flares and Coronal Mass Ejections (CMEs) (Bastian et al. 1998; Raulin & Pacini 2005; Gopalswamy 2009; White 2024). Among the various spectral classes, Type II bursts are of particular interest for space weather forecasting, as they are generated by magnetohydrodynamic (MHD) shocks often driven by CMEs, whereas Type III bursts trace the rapid travel of energetic electrons along open magnetic field lines (Cairns 2010; White 2024; Gopalswamy et al. 2008). These radio emissions, ranging from meter to decimeter wavelengths, serve as early warnings for geomagnetic storms and Solar Energetic Particle (SEP) events that can impact Earth’s magnetosphere (Ameri et al. 2019; Vourlidas et al. 2020; Maia et al. 1999).

To monitor these transient events continuously, the Compound Astronomical Low cost Low frequency Instrument for Spectroscopy and Transportable Observatory (CALLISTO) network was estab-

lished (Benz et al. 2005, 2009). Comprising more than 150 stations worldwide, this network utilizes low-cost programmable heterodyne receivers to observe dynamic solar radio events in the 45–870 MHz frequency range, generating spectra of a massive archive of Flexible Image Transport System (FITS) files<sup>1</sup> (Benz et al. 2009; Bussons Gordo et al. 2023). Although this extensive coverage is invaluable, the sheer volume of data, thousands of files per station annually, presents a significant analysis bottleneck (Singh et al. 2019). Raw spectra are frequently contaminated by terrestrial Radio Frequency Interference (RFI) and background noise, requiring robust filtering and processing techniques before meaningful physical parameters can be extracted (Hamidi & Shariff 2014).

In recent years, various computational methods and software tools have been developed to address these challenges, though they often suffer from limitations in accessibility, accuracy, or functional scope. Statistical approaches, such as the method proposed by Singh et al. (2019) using the Area Slope Index (ASI), attempt to distinguish bursts from noise automatically. However, these methods are often insensitive to weak bursts with low Signal-to-Noise Ratios (SNR <

\* E-mail: sahanlst@gmail.com, janaka@phys.cmb.ac.lk

<sup>1</sup> <https://www.e-callisto.org/Data/data.html>

$5\sigma$ ) and lack the capability to classify specific burst types accurately (Singh et al. 2019). Similarly, the "Burst-Finder" algorithm developed by Afandi et al. (2020) utilizes thresholding on resized spectra to detect bursts. While achieving a high detection rate, such fully automated systems are prone to false positives caused by RFI and are designed primarily for event logging rather than detailed physical analysis (Afandi et al. 2020).

More recently, deep learning approaches have been applied to e-CALLISTO data. For instance, Bussons Gordo et al. (2023) introduced the "deARCE" method based on Convolutional Neural Networks (CNNs) like AlexNet. While these "black box" models are highly effective for binary classification (burst vs. no-burst) and generating event reports, they require massive training datasets and do not provide the interactive environment necessary for researchers to extract precise kinematic properties of the shock waves (Bussons Gordo et al. 2023). On the other hand, libraries such as 'pyCallisto' offer Python-based functions for background subtraction and flux integration (Pawase & Raja 2020). However, 'pyCallisto' is a code library rather than a standalone application, requiring users to possess programming proficiency to script their own analysis pipelines, which creates a barrier for observational astronomers who require ready-to-use tools (Pawase & Raja 2020).

Attempts to bridge the gap between automation and interactivity include the "Solar Radio Burst Analyzer" developed by Hettiarachchi et al. (2024). This Python-based Graphical User Interface (GUI) assists in calculating drift rates using an "Intensity Matrix" method. Despite its utility, the software has notable limitations. First, it is semi-automated, relying heavily on the user to manually define start and end coordinates to isolate burst regions (Hettiarachchi et al. 2024). Second, it imposes rigid mathematical models on the data, assuming a linear fit for Type III bursts and an exponential decay model ( $f = ae^{-(b+t)/t} + c$ ) for Type II bursts (Hettiarachchi et al. 2024). These assumptions may fail to capture the complex, non-linear morphological variations often observed in dynamic solar eruptions. Furthermore, e-CALLISTO observations are segmented into 15-minute files; long-duration events often span multiple files, yet existing tools often lack a seamless workflow to merge these fragmented segments into a continuous spectrum for uninterrupted analysis (Benz et al. 2009; Pawase & Raja 2020). Due to the non-availability of the comprehensive analysis tool, some of the studies were limited to a few data files (Ansor et al. 2020; Wijesekera et al. 2018) despite the vast archive of e-CALLISTO. Furthermore, the e-CALLISTO archive consist of data from different locations, which may not identical in frequency span due to their ideal observation window within 45 - 870 MHz. Therefore, it is not easy to combine the fragmented radio bursts in two consecutive data files for the analysis Giersch et al. (2017).

To address these deficiencies, we present the "e-CALLISTO FITS Analyzer." Unlike the rigid modeling of Hettiarachchi et al. (2024) or the code-heavy nature of 'pyCallisto' (Pawase & Raja 2020), this new tool offers a flexible, unified GUI environment. It streamlines the ingestion of fragmented FITS files, automates file merging across time, and implements robust background subtraction to mitigate RFI. By providing interactive tools that allow for flexible tracking of burst backbones without restricting the user to specific mathematical shapes, the software facilitates the precise extraction of frequency drift rates and shock parameters. This tool aims to democratize access to rigorous solar radio analysis, enabling broader participation in space weather research.

The remainder of this paper is organized as follows: Section 2 describes the properties of e-CALLISTO data. Section 3 details the software architecture and methodology. Section 4 demonstrates the

analysis workflow using Type II bursts, and Section 5 concludes with a summary of the tool's capabilities.

## 2 E-CALLISTO SOLAR RADIO OBSERVATIONS

Solar radio dynamic spectra provide a direct view of transient energy release in the low and middle corona, where particle beams, shocks, and evolving magnetic structures generate coherent emission over metric and decametric wavelengths (Behlke 2001). The CALLISTO was developed as a compact, low-cost solar radio spectrometer that can be deployed widely, including at sites where access to large radio facilities is limited (Benz et al. 2005). The global deployment of many CALLISTO instruments forms the e-CALLISTO network<sup>2</sup>, designed as a space-weather instrument array with the aim of achieving near-continuous monitoring of solar radio activity through longitudinal coverage Monstein et al. (2023).

The significance of e-CALLISTO in spaceweather field arises from its ability to capture radio signatures associated with eruptive phenomena and particle acceleration, including Type II, Type III, and Type IV bursts Monstein (2011). Because these emissions can occur over short time scales and may be visible only from certain geographic longitudes at a given time, a distributed network improves event capture probability and supports operational monitoring and retrospective studies. The e-CALLISTO project also emphasizes broad accessibility, combining scientific use with education, outreach, and long-term radio-frequency-interference monitoring at participating sites (Monstein 2011).

### 2.1 CALLISTO solar radio spectrometer

CALLISTO is a programmable heterodyne receiver originally developed within the International Heliophysical Year and International Space Weather Initiative deployment framework, with an explicit focus on portability, low cost, and flexible observing programs (Dávila et al. 2007). The instrument is designed to repeatedly sweep through a user-defined set of frequency channels and record intensity as a function of time and frequency, producing dynamic spectra suitable for burst detection and analysis (Benz et al. 2005).

In its standard configuration, CALLISTO operates in the metric range, with nominal coverage between approximately 45 and 870 MHz using a broadband tuner architecture (Benz et al. 2005, 2009; Zucca et al. 2012). The observing program typically samples on the order of a few hundred channels per sweep, and the published network description reports a time resolution of about 0.25 s for spectra configured with 200 channels, together with a frequency resolution set by the receiver chain and channel spacing (Benz et al. 2009; Zucca et al. 2012). Benz et al. (2005) note millisecond-scale integration and an overall dynamic range exceeding tens of decibels, which is sufficient for capturing both weak and intense burst features in routine monitoring. A practical strength of CALLISTO is its configurability. Frequency channel lists can be defined to avoid persistent interference and target bands of interest, while optional frequency conversion hardware can extend the accessible range beyond the native tuner limits (Benz et al. 2005). This flexibility is central to network operation because it allows stations in different radio environments to tune their observing schedules and frequency plans while still producing standardized dynamic spectra products for the common archive (Rusu et al. 2015).

<sup>2</sup> <https://www.e-callisto.org/>

## 2.2 Data from CALLISTO

CALLISTO observations are stored as FIT-compatible “FIT” files and are commonly distributed in compressed form in the network archive. The network documentation summarizes the data product as a dynamic spectrum, where the horizontal axis is the time in UT, the vertical axis is the frequency in MHz, and the pixel values represent the instrument intensity in arbitrary digital units (ADU) (Adassuriya et al. 2023).

The CALLISTO operating manual describes each FITS file as comprising a primary header followed by the binary spectrogram data and two binary table components that encode the time axis and the frequency axis. This structure supports reliable reconstruction of the spectrogram in external analysis software because the axis information is carried along the intensity matrix, rather than being implied by filename conventions alone.

In routine operation, data are written locally at the station and then uploaded to the central archive infrastructure. The e-CALLISTO site describes automated transfer of data from individual instruments to a central server and provides multiple access modes, including original FIT files, quicklook products, and derived daily overviews and light curves.

Archive naming conventions and quicklook products are designed to preserve essential provenance, including station identity and acquisition time. For example, the quicklook dataset documentation uses filenames of the form STATION\_YYYYMMDD\_HHMMSS\_CODE\_fit.gz, which encodes the station name, observation date, start time, and an additional instrument/front-end descriptor. Such conventions simplify automated indexing and allow users to retrieve the corresponding raw FIT file for any plotted quicklook interval.

## 3 SOFTWARE IMPLEMENTATION AND PROCESSING WORKFLOW

### 3.1 Data model and FITS handling

The application adopts an in-memory representation that maps naturally to a solar radio dynamic spectrum. After import, each observation is modeled as a two-dimensional intensity matrix

$$I \in \mathbb{R}^{N_f \times N_t}, \quad (1)$$

where rows correspond to frequency channels and columns correspond to time samples. Two one-dimensional vectors define the coordinate system: the frequency vector  $\{f_i\}_{i=1}^{N_f}$  (in MHz) and the time vector  $\{t_j\}_{j=1}^{N_t}$  (in seconds). This representation is preserved across the entire workflow so that background removal, masking, and merging are expressed as well-defined operations on arrays with fixed axis semantics.

FITS files are parsed according to common e-CALLISTO conventions, in which the intensity matrix is stored in the primary data unit and the auxiliary coordinate information is provided through associated metadata and table content. The insertion pipeline supports both uncompressed FITS files and gzip-compressed FITS products, enabling the use of original station output as well as compressed archival products. When available, observation timing metadata are extracted from the FITS header to define an absolute reference time for later UT formatting (Figure: 1).

### 3.2 Data acquisition and insertion

Data enter the processing pipeline through either local file selection or the integrated downloader (Figure: 2). In both cases, the objective

is to obtain a validated set of FITS inputs, extract the core arrays  $(I, f, t)$ , and populate the main plotting context while maintaining interactive responsiveness.

For remote acquisition, the downloader queries an archive directory for a user-selected date and filters the listing using station identifiers and time information encoded in filenames. Transfers are executed in a background worker so that the graphical interface remains responsive during network activity. Before import, an initial preview can be rendered to help confirm the station, time interval, and spectral coverage. Upon confirmation, the selected files are downloaded to a local workspace and passed through the same parsing path used for locally opened files, which ensures that subsequent processing and visualization are independent of the data source.

### 3.3 FITS combination across time and frequency

e-CALLISTO observations are commonly split across multiple FITS files, either to cover adjacent frequency sub-bands or to segment the observation into consecutive time intervals. To support event-level analysis, the application provides two combination modes that produce a single consolidated product  $(I, f, t)$  for downstream visualization and analysis. The workflow is shown in the Figure 3.

In frequency combination, multiple files that share compatible time sampling but provide different frequency sub-bands are merged to enlarge instantaneous spectral coverage. The intensity matrices are stacked along the frequency axis and the frequency vectors are concatenated accordingly, while the time vector is preserved. For two compatible files, this can be written as

$$I_{\text{freq}} = \begin{bmatrix} I^{(1)} \\ I^{(2)} \end{bmatrix}, \quad f_{\text{freq}} = \begin{bmatrix} f^{(1)} \\ f^{(2)} \end{bmatrix}, \quad t_{\text{freq}} = t. \quad (2)$$

This operation is important when bursts extend across a wide band and a single receiver setting does not capture the full frequency extent of the emission.

In time combination, files from the same station and receiver configuration are merged to extend the observation duration. The intensity matrices are concatenated along the time axis. Since individual segments often carry a time vector that restarts near zero, each segment is shifted by a cumulative offset so that the combined time axis is monotonic and continuous. With  $K$  consecutive segments, the merged product is

$$I_{\text{time}} = [I^{(1)} \ I^{(2)} \ \dots \ I^{(K)}], \quad t_{\text{adj}}^{(k)} = t^{(k)} + \Delta_k, \quad (3)$$

where  $\Delta_k$  is the accumulated duration of all previous segments. Time merging is particularly relevant for Type II and Type III bursts that span multiple acquisition blocks, allowing a single continuous dynamic spectrum to be used for isolation and measurement.

### 3.4 background subtraction and burst isolation

background subtraction is designed to suppress quasi-stationary background structure while preserving transient burst signatures. Let  $I_{i,j}$  denote the intensity at frequency index  $i$  and time index  $j$ . A per-frequency baseline is estimated as a mean over time,

$$\mu_i = \frac{1}{N_t} \sum_{j=1}^{N_t} I_{i,j}, \quad (4)$$

and the background-subtracted matrix is computed as

$$\tilde{I}_{i,j} = I_{i,j} - \mu_i. \quad (5)$$

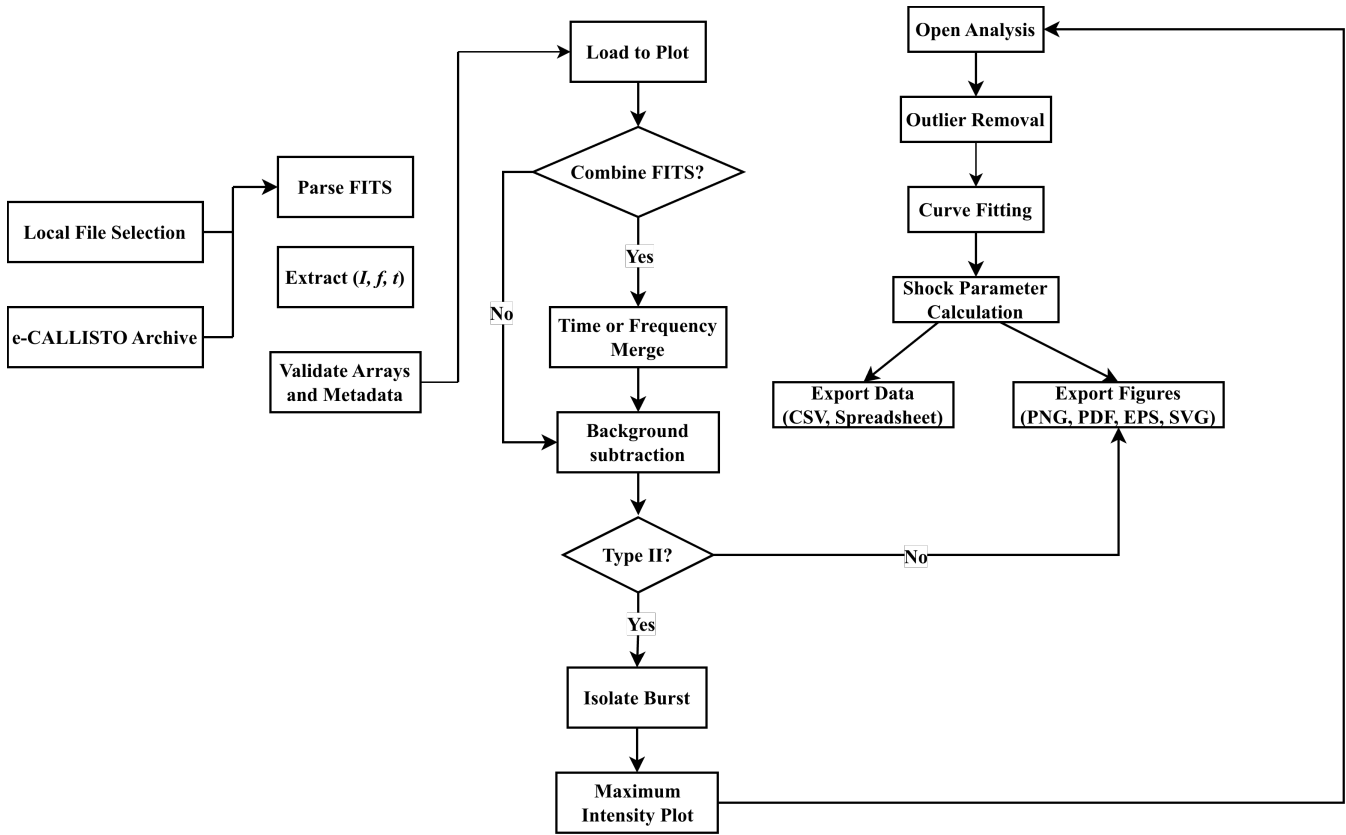


**Figure 1.** Overall workflow of the e-Callisto FITS Analyzer.

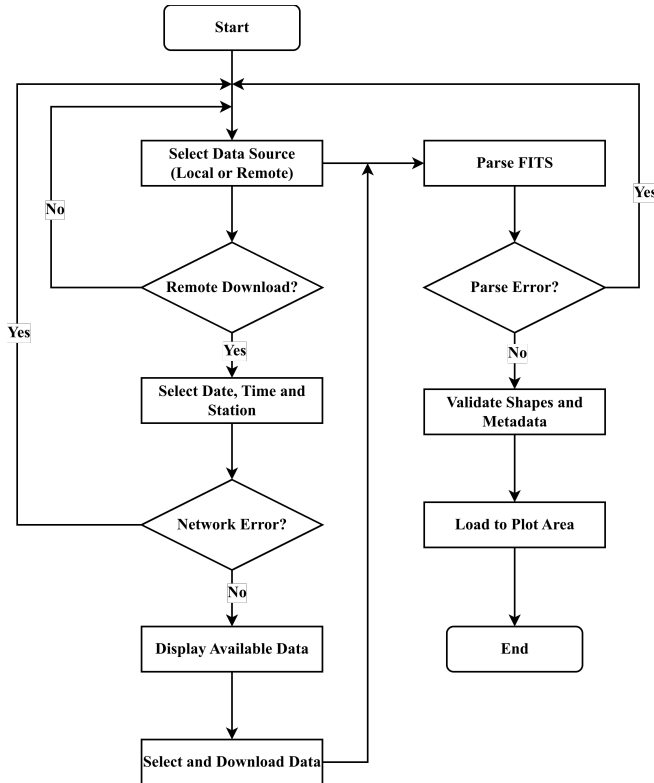


**Figure 2.** Data acquisition workflow of the e-Callisto FITS Analyzer.

This operation reduces persistent offsets and band-dependent structure while retaining time-varying emission (Liyanage et al. 2025).

After subtraction, the application applies user-controlled clipping thresholds to reduce residual background and emphasize burst morphology. For lower and upper thresholds ( $L$ ,  $H$ ), the clipped intensity is

$$I_{i,j}^* = \min(\max(\tilde{I}_{i,j}, L), H). \quad (6)$$

Thresholds can be adjusted interactively so that users can tune contrast without reloading data. Optional display scaling may be applied for visualization, but the internal matrix structure remains consistent throughout the analysis (Liyanage et al. 2025).

Burst isolation is implemented as an interactive masking operation in the time–frequency plane. A user-defined closed region is traced around the feature of interest, producing a polygon  $P$  in plot coordinates. This region is mapped onto the discrete grid to form a Boolean mask  $M \in \{0, 1\}^{N_f \times N_t}$ ,

$$M_{i,j} = \begin{cases} 1, & (t_j, f_i) \in P, \\ 0, & \text{otherwise.} \end{cases} \quad (7)$$

The isolated burst product is then computed by elementwise masking,

$$I_{iso} = M \odot I^*, \quad (8)$$

where  $\odot$  denotes the Hadamard product. Pixels outside the selected region are suppressed, yielding a burst-only matrix that can be used for subsequent quantitative analysis. This approach is agnostic to burst class and supports isolation of Type II lanes, Type III streaks, and more complex multi-component structures, provided they can be enclosed in the time-frequency plane.

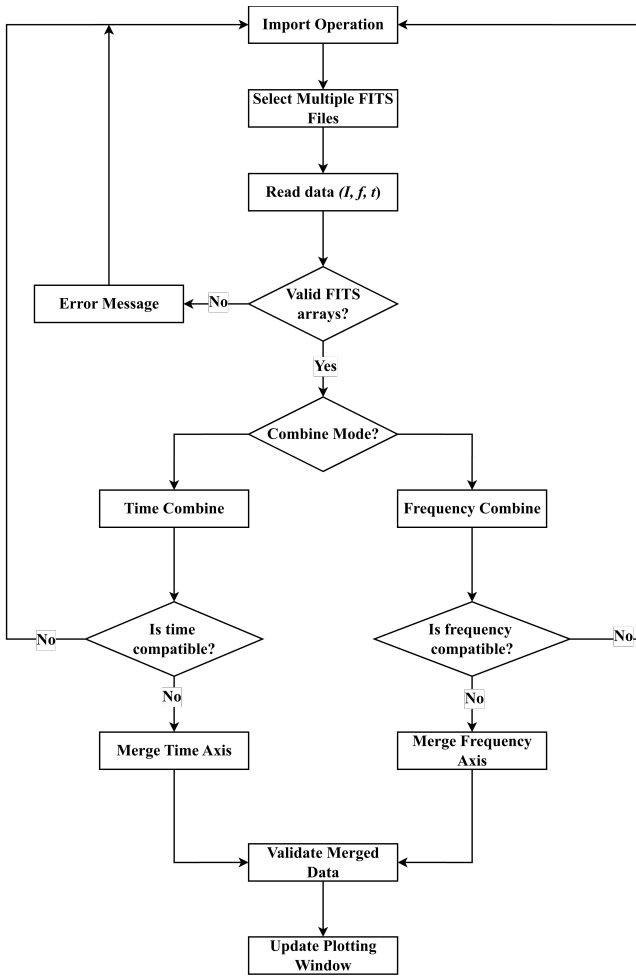


Figure 3. The FITS combination workflow for Time and Frequency merge.

### 3.5 Data visualization

Visualization is built on an embedded plotting canvas that renders the dynamic spectrum as a two-dimensional image with physically meaningful axes. The intensity matrix is displayed using an extent that maps matrix indices onto the time and frequency vectors, so cursor readout and interactive selections operate in seconds and MHz rather than pixel coordinates.

Time labeling can be expressed either as elapsed seconds or as UT. When UT mode is enabled, an observation start time  $t_0$  extracted from FITS metadata is used to format displayed time as

$$t_{\text{UT}} = t_0 + t. \quad (9)$$

Color scaling is managed through a dedicated colorbar axis and a selectable colormap, enabling consistent inspection across raw, background-subtracted, and isolated-burst views. The visualization layer separates data state from display state so that plot updates can be performed without discarding the user’s current view limits.

### 3.6 User interaction and control layer

The user interaction layer is designed to support rapid, iterative exploration. Background suppression thresholds are exposed through continuous controls and applied directly to the in-memory representation, enabling immediate feedback during tuning. Standard zooming and panning interactions allow users to focus on specific time–

frequency regions, and view limits can be preserved across plot refreshes so that users maintain spatial context while adjusting thresholds, colormaps, or axis formatting.

Interactive isolation tools are integrated into the same plotting context so that selection and visualization remain consistent. The cursor readout provides time, frequency, and intensity values at the pointer location, supporting manual inspection of burst lanes. To support iterative analysis, the application maintains an undo and redo history that captures both data-state changes and view state, which reduces friction when exploring multiple parameter choices.

### 3.7 Extensibility and modular design

The software is structured as modular components that share a common graphical framework while remaining loosely coupled at the data level. The core radio pipeline focuses on FITS insertion, cleaning, visualization, and burst isolation. Space-weather context products are integrated as separate modules launched from the main interface. GOES X-ray flux visualization is implemented as a dedicated component that retrieves and plots time-series data, while SOHO/LASCO CME browsing is provided through an independent viewer tailored to catalog access and event inspection.

This modular organization supports extension in two directions. First, the radio analysis workflow can remain stable while new context modules are added. Second, each external data stream can evolve its own parsing, caching, and plotting logic without forcing changes to FITS handling or the radio processing pipeline.

### 3.8 Software dependencies and environment

The application is implemented in Python and relies on established scientific and graphical libraries to enable cross-platform execution, FITS I/O, interactive visualization, numerical processing, and access to external space-weather resources. Dependencies were selected to balance stability, performance, and maintainability, while keeping installation practical for end users (Table: 1).

For reproducibility, analysis can be accompanied by a record of the computational environment used to generate exported figures and derived data products. This is typically achieved by archiving a dependency manifest or an environment specification alongside the processed dataset and manuscript materials.

Apart from that, the e-CALLISTO FITS Analyzer natively works on Windows, macOS and Linux(Debian/Ubuntu) and native installers are available to download and use via the official e-CALLISTO website<sup>3</sup>. Also, the source code is published at GitHub<sup>4</sup>.

### 3.9 Design considerations and limitations

Several design choices prioritize interactive research use while maintaining clear separation between data transformations and visualization. The application maintains a single canonical in-memory representation of the spectrum, and plot refreshes are derived from this state so that processing steps remain traceable. Network activity is delegated to worker threads to avoid blocking the interface, and plotting updates are managed through the GUI event loop to reduce instability during interactive sessions.

The methodology also imposes practical limitations. Combination across time and frequency depends on compatibility assumptions that

<sup>3</sup> <https://www.e-callisto.org/Software/Callisto-Software.html>

<sup>4</sup> [https://github.com/SaanDev/e-Callisto\\_FITS\\_Analyzer](https://github.com/SaanDev/e-Callisto_FITS_Analyzer)

**Table 1.** Principal software dependencies and their roles. Versions should be reported from the reference environment used in the experiments.

Dependency	Role in the software	Version used
Python	Runtime environment	3.13.4
PySide6	Desktop GUI framework and Qt bindings	6.10.1
NumPy	Array model and numerical operations on spectra	2.3.5
Matplotlib	Embedded plotting, colormaps, interaction, and figure export	3.10.7
PyQtGraph	High-performance plotting	0.14.0
Astropy	FITS input/output, header handling, and astronomy data utilities	7.2.0
SciPy	Numerical utilities used in analysis routines	1.16.3
OpenPyXL	Spreadsheet export	3.1.5
Requests	HTTP retrieval for remote data sources and update checks	2.32.5
BeautifulSoup4	HTML parsing for server listings and catalogs	4.14.3
netCDF4	GOES data insertion	1.7.3
cftime	Time handling for netCDF and GOES products	1.6.5
SunPy	Multi-mission solar archive query, download, plotting, and analysis	7.1.0
scikit-learn	Optional analysis utilities where applicable	1.7.2
setuptools	Build and distribution support	80.9.0

generally hold for standard e-CALLISTO products but may fail for atypical station configurations or inconsistent acquisition settings. Time merging constructs a continuous axis through cumulative offsets and does not, by itself, guarantee correction for gaps, overlaps, or station clock irregularities. Frequency merging assumes compatible time sampling across selected files, and reliability depends on consistency in metadata and file naming conventions.

background subtraction is intentionally model-light. Mean background subtraction and threshold clipping perform well for many burst morphologies but can suppress weak diffuse emission and may alter the apparent intensity distribution when the background varies rapidly. Burst isolation depends on a user-defined region and on the mapping between continuous plot coordinates and the discrete data grid, which can introduce selection sensitivity near burst boundaries. Finally, any display scaling used for visualization should not be interpreted as full radiometric calibration unless station-specific calibration metadata and procedures are explicitly incorporated.

## 4 ANALYSIS OF TYPE II BURSTS

Type II solar radio bursts provide one of the most direct radio diagnostics of coronal shock propagation (Mann et al. 1995). In dynamic spectra, they appear as slowly drifting lanes that trace the plasma frequency (or its harmonic) as the shock traverses decreasing coronal density (Tsap et al. 2020). Quantifying the lane trajectory therefore enables physically meaningful parameters to be inferred, including the frequency drift rate, shock formation height, and shock speed under an assumed coronal density model (Late AA Weiss 1965; Gopalswamy et al. 2013). In metric observations, Type II bursts often show both a fundamental band and a harmonic band. The fundamental emission is expected near the local plasma frequency  $f_{pe}$ , while the harmonic emission occurs near  $2f_{pe}$  (Cane & Erickson 2005). In the present workflow, calculations are performed using the fundamental band whenever it is sufficiently clear. When the fundamental lane is weak, fragmented, or obscured, the harmonic lane can be selected and converted to the equivalent fundamental frequency by  $f_{pe} \approx f_H/2$  prior to physical parameter estimation. This selection is performed directly in the analyzer interface, allowing the measurement to remain consistent with the visible lane morphology.

### 4.1 Maximum-intensity backbone after isolation

After performing background subtraction and isolating the burst, the next step in the analysis is to obtain a one-dimensional representation of the burst that reflects how its characteristic frequency changes over time. The application creates this representation by extracting a backbone curve from the isolated intensity matrix. Let  $I \in \mathbb{R}^{N_f \times N_t}$  be the processed spectrum and  $M \in \{0, 1\}^{N_f \times N_t}$  be the isolation mask, where  $M_{i,j} = 1$  for pixels that remain within the chosen burst region. For each time index  $j$ , the backbone is defined by selecting the frequency index that maximizes the intensity after masking:

$$i^*(j) = \arg \max_i (M_{i,j} I_{i,j}), \quad f_{\max}(t_j) = f_{i^*(j)}. \quad (10)$$

This procedure converts the two-dimensional burst structure into a single curve  $f_{\max}(t)$  that follows the most intense ridge of emission at each time step (Liyanage et al. 2025). The maximum-intensity backbone is well suited to Type II analysis because the lane is often band-limited but not infinitesimally thin, and the local intensity maximum provides a practical proxy for the lane center even when the emission is broadened by instrumental response, scattering, or fine structure.

Residual artifacts may still appear as outliers in the extracted backbone. These outliers commonly arise from incomplete suppression of radio-frequency interference, leakage from the harmonic lane, or isolated bright pixels remaining after clipping. Instead of relying solely on automatic heuristics, the tool provides an interactive outlier removal step in which the user selects spurious points directly on the backbone plot and removes them immediately. This interaction is particularly effective because outliers are typically separated geometrically from the smooth lane trend in the  $(t, f)$  plane, and manual selection preserves scientifically meaningful points that may be rejected by overly aggressive automated filters. The cleaned backbone then forms the input to parametric fitting and drift-rate estimation.

### 4.2 Frequency drift-rate calculation

The frequency drift rate is a key observable of Type II bursts because it encodes the rate at which the shock-driven emission region moves through the coronal density gradient. After outlier removal, the backbone points are fitted using a power-law model,

$$f(t) = A t^b, \quad (11)$$

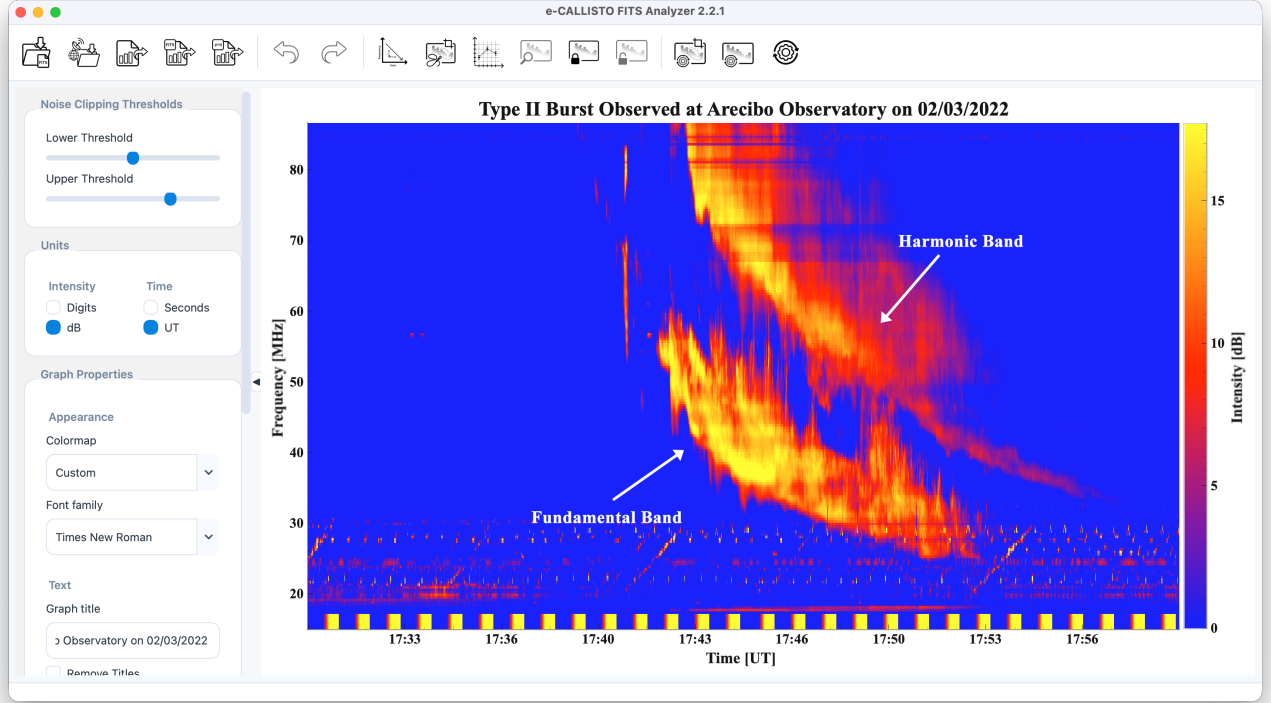


**Figure 4.** The main application window showing a Type II solar radio burst observed at Arecibo Observatory on 2 March 2022 after background subtraction.

where  $A$  and  $b$  are fitting parameters and  $t$  denotes the elapsed time along the selected burst segment (Liyanage et al. 2025). The instantaneous drift rate is obtained from the derivative of the fitted curve,

$$\frac{df}{dt} = A b t^{(b-1)}. \quad (12)$$

Since Type II lanes may exhibit short-scale irregularities even after cleaning, the application reports an average drift rate that summarizes the overall lane trend across the selected interval. If the fitted curve is evaluated at  $N$  time samples  $\{t_j\}$ , the mean absolute drift rate can be expressed as

$$\bar{D} = \frac{1}{N} \sum_{j=1}^N \left| \frac{df}{dt} \Big|_{t=t_j} \right|. \quad (13)$$

This approach reduces sensitivity to local measurement noise while preserving the physically relevant monotonic drift of the Type II burst (Liyanage et al. 2025).

### 4.3 Shock-parameter estimation

To determine the coronal shock parameters the measured drift rate and electron density model  $n_e(R)$  have been used. Under the one-fold Newkirk density model, the coronal electron density varies with heliocentric distance  $R$  as

$$n_e(R) = n_0 10^{\alpha (R_\odot/R)}, \quad (14)$$

where  $n_0 = 4.2 \times 10^4 \text{ cm}^{-3}$  is the electron density near to the solar surface,  $\alpha = 4.32$  is a fitting constant, and  $R_\odot = 696340 \text{ km}$  is the solar radius (Newkirk 1961). The plasma frequency can be written

in MHz as

$$f_{pe} = \kappa \sqrt{n_e}, \quad (15)$$

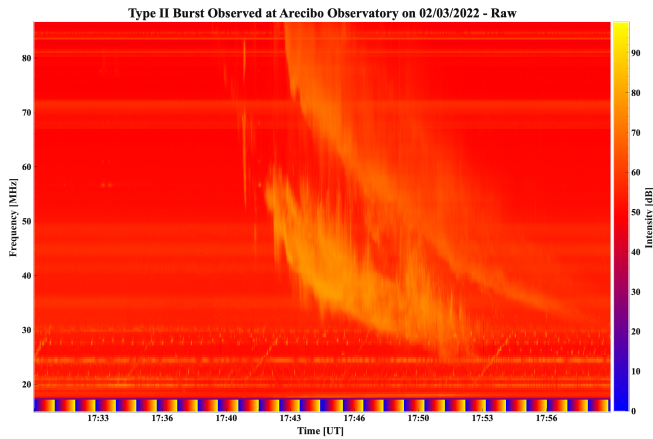
where  $\kappa \approx 8.978 \times 10^{-3} \text{ MHz cm}^{-\frac{3}{2}}$  is a constant that collects physical constants and unit conversions (Nicholson 1983). Combining the density model with the plasma-frequency relation yields an explicit expression for the shock source height  $R_s$  as a function of plasma frequency (Liyanage et al. 2025):

$$R_s = \frac{\alpha R_\odot \ln(10)}{\ln\left(\frac{f_{pe}^2}{n_0 \kappa^2}\right)} \quad (16)$$

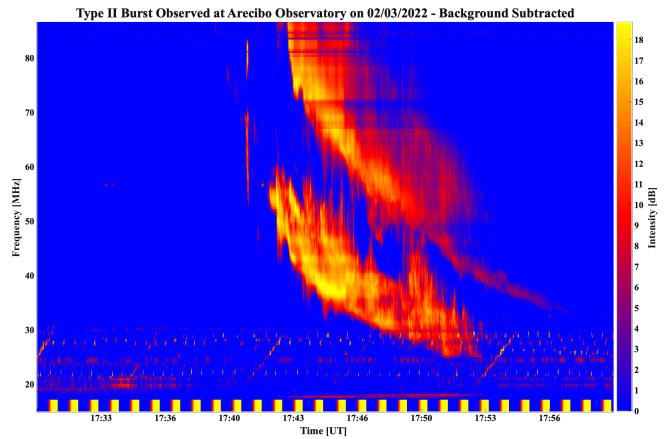
Differentiating this expression with respect to time gives the shock speed  $V_s = dR_s/dt$ , which can be written in terms of the frequency drift rate (Liyanage et al. 2025):

$$V_s = \frac{2\alpha R_\odot \ln(10)}{f_{pe} \ln^2\left(\frac{f_{pe}^2}{n_0 \kappa^2}\right)} \left| \frac{df_{pe}}{dt} \right| \quad (17)$$

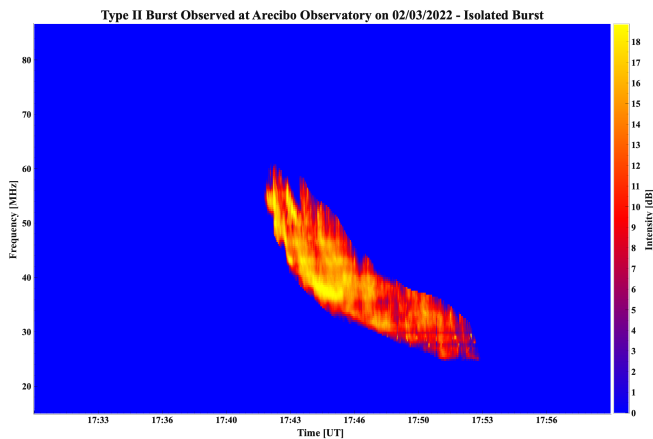
In the application,  $f_{pe}$  is taken from the selected band. For a fundamental band, the observed band frequency is treated as  $f_{pe}$ . For a harmonic band, the plasma frequency is inferred by  $f_{pe} \approx f_H/2$ , and the corresponding drift rate is considered as same as the fundamental band. The drift rate is obtained from the fitted derivative, while the source height is estimated from the starting frequency (for example, a starting-frequency estimate derived from the upper portion of the band). These steps produce a self-consistent set of shock parameters tied directly to the user-verified band morphology.



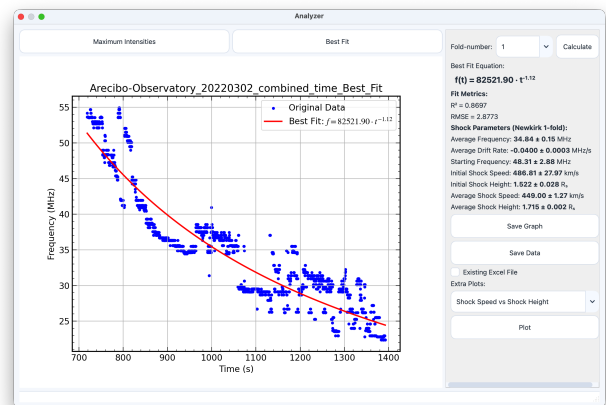
(a) Raw dynamic spectrum of the Type II solar radio burst recorded by the CALLISTO instrument at Arecibo Observatory on 02/03/2022.



(b) Background subtracted dynamic spectrum of the Type II solar radio burst recorded by the CALLISTO instrument at Arecibo Observatory on 02/03/2022.



(c) Isolated fundamental band of dynamic spectrum of the Type II solar radio burst recorded by the CALLISTO instrument at Arecibo Observatory on 02/03/2022.



(d) Analyzer window showing the maximum-intensity backbone and the derived shock parameters for the same burst, calculated using the one-fold Newkirk electron density model.

**Figure 5.** Processing stages of the e-CALLISTO FITS Analyzer for a Type II solar radio burst observed by CALLISTO at Arecibo Observatory on 02/03/2022: (a) raw dynamic spectrum, (b) background-subtracted dynamic spectrum, (c) isolated fundamental band, and (d) analyzer window showing the maximum-intensity backbone and derived shock parameters computed using the one-fold Newkirk electron density model.

#### 4.4 Example Application of the Tool

A typical analysis begins by loading a metric e-CALLISTO FITS observation, either from local storage or by downloading the relevant files from the archive and importing them into the main window. The dynamic spectrum is first inspected in its raw form to verify the time interval and frequency coverage (Figure 5a). The user then applies background subtraction and intensity clipping to reduce persistent spectral structure and enhance burst contrast (Figure 5b). Once the Type II emission is visible, the lasso tool is used to isolate the relevant lane region. At this stage, the user chooses whether to isolate the fundamental band or, when necessary, the harmonic band, based on which band is most reliably traceable (Figure 5c).

The isolated spectrum is then converted into a fitted curve by extracting the maximum-intensity frequency at each time sample within the selected region. The resulting  $f_{\max}(t)$  curve is displayed in the maximum-intensity window, where outliers can be removed interactively by selecting and deleting those points. With the cleaned maximum intensity plot, the analyzer performs a power-law fit and evaluates the derivative of the fitted function to obtain drift-rate

estimates and an average drift rate over the selected interval. Finally, the tool computes the shock source height and shock speed using the adopted density model and the measured frequency and drift rate, and provides publication-ready exports of plots and tabulated outputs for documentation and further statistical analysis (Figure 5d).

## 5 CONCLUSIONS

This work introduces the e-CALLISTO FITS Analyzer as a practical framework for processing and analyzing e-CALLISTO FITS dynamic spectra in a single GUI environment. The application addresses common bottlenecks in solar radio burst studies by streamlining FITS ingestion, supporting archive download with preview, and providing robust mechanisms to merge fragmented observations across time and frequency into a continuous spectrum suitable for event-level analysis.

The core processing workflow combines model-light background subtraction with interactive control. Mean background subtraction and threshold clipping reduce persistent band structure while allow-

ing the user to tune contrast without reloading data, and polygon-based masking enables burst isolation without imposing a rigid burst geometry. For Type II bursts, the analyzer extends this interactive approach into quantitative measurements by extracting a maximum-intensity backbone, allowing point-wise outlier removal, fitting a power-law model to estimate drift rates, and converting these measurements into shock parameters under an adopted coronal density model.

The software is designed to remain extensible. In addition to the radio pipeline, space-weather context modules are integrated as separate components, including GOES X-ray flux visualization and SOHO/LASCO CME browsing, enabling event inspection within the same application ecosystem while keeping the radio workflow stable.

Several limitations remain and also guide future development. Time and frequency merging depend on compatibility assumptions and do not automatically correct gaps, overlaps, or station timing irregularities. background subtraction, while effective for many cases, can suppress weak diffuse emission when the background varies rapidly, and burst isolation still depends on user-defined regions. Future work will focus on improving robustness for heterogeneous station configurations, adding more automated assistance for burst candidate selection while retaining user control, and expanding physical analysis options such as additional density models and calibration-aware products for studies that require absolute intensity interpretation.

## 6 ACKNOWLEDGEMENTS

We thank the Fachhochschule Nordwestschweiz (FHNW), Institute for Data Science in Brugg/Windisch, Switzerland, for hosting the e-CALLISTO network. The authors also acknowledge the efforts of individual CALLISTO operators, including the Arecibo Observatory, Puerto Rico. The Arecibo Observatory was operated by the University of Central Florida under a cooperative agreement with the National Science Foundation (AST-1822073). We gratefully acknowledge the Department of Physics, University of Colombo, and the Astronomical and Space Science Unit for providing the resources and institutional support that made this work possible.

## REFERENCES

Adassuriya J., Gunasekera S., Jayaratne K., Monstein C., 2023, arXiv preprint arXiv:2308.01581

Afandi N., Sabri N., Umar R., Monstein C., 2020, *Indian Journal of Physics*, 94, 947

Ameri D., Valtonen E., Pohjolainen S., 2019, *Solar Physics*, 294, 122

Ansor N. M., Hamidi Z. S., Shariff N. N. M., 2020, *Int. J. Recent Technol. Eng. (IJRTE)*, 9

Bastian T., Benz A., Gary D., 1998, *Annual Review of Astronomy and Astrophysics*, 36, 131

Behlke R., 2001, *IRF Scientific Report 275*

Benz A. O., Monstein C., Meyer H., 2005, *Solar Physics*, 226, 143

Benz A., et al., 2009, *Earth, Moon, and Planets*, 104, 277

Bussons Gordo J., Fernández Ruiz M., Prieto Mateo M., Alvarado Díaz J., Chávez de la O F., Ignacio Hidalgo J., Monstein C., 2023, *Solar Physics*, 298, 82

Cairns I. H., 2010, *The Sun, the solar wind, and the heliosphere*, pp 267–338

Cane H., Erickson W., 2005, *The Astrophysical Journal*, 623, 1180

Davila J., Gopalswamy N., Haubold H. J., Thompson B., 2007, *Space Policy*, 23, 121

Giersch O., Kennewell J., Lynch M., 2017, *Space Weather*, 15, 1511

Gopalswamy N., 2009, in *Climate and Weather of the Sun-Earth System (CAWSES): Selected Papers from the 2007 Kyoto Symposium*.

Gopalswamy N., Yashiro S., Akiyama S., Mäkelä P., Xie H., Kaiser M., Howard R., Bougeret J., 2008, in *Annales Geophysicae*. pp 3033–3047

Gopalswamy N., et al., 2013, *Advances in Space Research*, 51, 1981

Hamidi Z., Shariff N., 2014, *International Letters of Chemistry, Physics and Astronomy*, 15

Hettiarachchi Y., Adassuriya J., Jayaratne C., Jayawardhana S., Monstein C., 2024, *New Astronomy*, 109, 102194

Late AA Weiss T., 1965, *Australian Journal of Physics*, 18, 167

Liyanage G., Adassuriya J., Jayaratne K., Monstein C., 2025, in *Proceedings of the Technical Sessions*. pp 59–67

Maia D., Pick M., Vourlidas A., Howard R., 1999, *The Astrophysical Journal*, 528, L49

Mann G., Classen T., Aurass H., 1995, *Astronomy and Astrophysics*, v. 295, p. 775, 295, 775

Monstein C., 2011, *Phys Astron Electron Work Bench*

Monstein C., Csillaghy A., Benz A. O., 2023, *CALLISTO Quick-look Solar Spectrogram Plots*, doi:10.48322/WY0B-TQ35, <https://spase-metadata.org/ISWI/DisplayData/Callisto/FAS/PT15M>

Newkirk Jr. G., 1961, *ApJ*, 133, 983

Nicholson D. R., 1983, *Introduction to Plasma Theory*. John Wiley & Sons, New York

Pawase R., Raja K. S., 2020, *pyCallisto: A Python Library To Process The CALLISTO Spectrometer Data* (arXiv:2006.16300), <https://arxiv.org/abs/2006.16300>

Raulin J.-P., Pacini A., 2005, *Advances in Space Research*, 35, 739

Russu A., Gómez-Herrero R., Prieto M., Monstein C., Ivanov H., Rodríguez-Pacheco J., Blanco J., 2015, *Journal of Physics: Conference Series*, 632

Singh D., Sasikumar Raja K., Subramanian P., Ramesh R., Monstein C., 2019, *Solar Physics*, 294, 112

Tsap Y. T., Isaeva E., Kopylova Y. G., 2020, *Astronomy Letters*, 46, 144

Vourlidas A., Carley E. P., Vilmer N., 2020, *Frontiers in Astronomy and Space Sciences*, 7, 43

White S. M., 2024, arXiv preprint arXiv:2405.00959

Wijsekera J., Jayaratne K., Adassuriya J., 2018, in *Journal of Physics: Conference Series*. p. 012046

Zucca P., Carley E., McCauley J., Gallagher P., Monstein C., McAteer R., 2012, *Solar Physics*, 280, 591

This paper has been typeset from a  $\text{\TeX}/\text{\LaTeX}$  file prepared by the author.